Polysulfide Flow Batteries Enabled by Percolating Nanoscale Conductor Networks

Citation: Fan, Frank Y., William H. Woodford, Zheng Li, Nir Baram, Kyle C. Smith, Ahmed Helal, Gareth H. McKinley, W. Craig Carter, and Yet-Ming Chiang. "Polysulfide Flow Batteries Enabled by Percolating Nanoscale Conductor Networks." Nano Lett. 14, no. 4 (April 9, 2014): 2210–2218.

As Published: http://dx.doi.org/10.1021/nl500740t

Publisher: American Chemical Society (ACS)

Persistent URL: http://hdl.handle.net/1721.1/101762

Version: Original manuscript: author's manuscript prior to formal peer review

Polysulfide Flow Batteries Enabled by Percolating Nanoscale Conductor Networks

Frank Y. Fan[1], William H. Woodford[1], Zheng Li[1], Nir Baram[1], Kyle C. Smith[1], Ahmed Helal[2], Gareth H. McKinley[2], W. Craig Carter[1], and Yet-Ming Chiang*[1]

Abstract

A new approach to flow battery design is demonstrated wherein diffusion-limited aggregation of nanoscale conductor particles at ~1 vol% concentration is used to impart mixed electronic-ionic conductivity to redox solutions, forming flow electrodes with embedded current collector networks that self-heal after shear. Lithium polysulfide flow cathodes of this architecture exhibit electrochemical activity that is distributed throughout the volume of flow electrodes rather than being confined to surfaces of stationary current collectors. The nanoscale network architecture enables cycling of polysulfide solutions deep into precipitation regimes that historically have shown poor capacity utilization and reversibility, and may thereby enable new flow battery designs of higher energy density and lower system cost. Lithium polysulfide half-flow cells operating in both continuous and intermittent flow mode are demonstrated for the first time.

[1]Department of Materials Science and Engineering, Massachusetts Institute of Technology, Cambridge, Massachusetts 02139, USA. [2]Department of Mechanical Engineering, Massachusetts Institute of Technology, Cambridge, Massachusetts 02139, USA

*corresponding author, email: ychiang@mit.edu

Renewable energy generation technologies such as wind and solar suffer from intermittency, while existing baseload nuclear and fossil fuel generation plants are most efficient and long-lived when operated at constant output. There exists an unmet need for low-cost efficient energy storage at gigawatt-hour scale capacity, either as large centralized plants or smaller units co-located with distributed generation, to facilitate the growth and integration of renewable energy. Flow batteries (Fig. 1) possess an attractive architecture for such storage due to their ability to decouple stored energy (the tanks) from power (the stack), inherent scalability, and potentially low cost[1]. Lowering the cost of stored energy below ~$100/kWh at system level remains a challenge, however[2,3]. Many aqueous solution-based flow battery chemistries are known, all of which have historically been used in some variant of the same basic flow cell architecture and operate at < 1.2 V cell voltage with ~1-2 M solution concentrations[4]. The electrode (often termed catholyte and anolyte in literature) is flowed through a current-extracting stack. Lower-cost, higher energy density (Wh/L) flow chemistries that decrease system size and associated hardware costs, and approaches that minimize or avoid use of high cost components such as ion-selective membranes, are desirable. Promising new approaches include semi-solid flow batteries using suspensions of solid storage compounds as flow electrodes[5–7], and several new classes of solution reactants including lithium polysulfide solutions[8,9], all-organic redox couples[10], and ionic liquid based complexes[11]. However, as energy density increases, several barriers to efficient extraction of electrochemical energy are inevitable. Increases in solution molarity, especially for large molecules facilitating high solubility, are accompanied by higher viscosities leading to higher driving pressures and greater flow resistance. Reaction rates will typically decrease, due to sluggish bulk diffusion or less facile interfacial reaction rates (i.e., Butler-

Volmer exchange current density). These sources of polarization are further compounded by the higher absolute current densities that are necessary to utilize higher volumetric energy at equivalent rate. All of the above tend to lower cell-level coulombic and energetic efficiency.

Here we demonstrate a new approach, broadly applicable to flowable redox chemistries—including those which undergo precipitation-dissolution reactions—whereby percolating networks of nanoscale conductor particles are incorporated within fluid electrodes forming an embedded, self-healing current collector enabling highly distributed electrochemical reactivity throughout the electroactive zone of flow batteries. In contrast to conventional flow battery designs wherein the electronically-insulating redox fluids undergo charge-transfer reactions only upon contact with the stationary porous current collector (Fig. 1c), the new scheme produces an electronically conductive fluid (i.e., a "liquid wire", Fig. 1d) that acts as its own current collector, providing for charge transfer to the external circuit. The continuous nanoconductor network vastly increases the available charge-transfer area while also reducing the molecular diffusion length between electroactive sites. As we show, in the high ionic strength environment of liquid electrolytes, nanoscale carbon conductor particles undergo diffusion-limited aggregation leading to electronic percolation at remarkably low volume concentrations of <1%, and reach 5-20 mS/cm electronic conductivity for only 1-3 vol% solids in non-aqueous electrolytes, providing excellent mixed electronic-ionic conduction with negligible impact on energy density. We use lithium-polysulfide (Li-PS) as a test system, and show that the new electrode architecture allows electrochemical utilization that is increased fivefold over the same solutions used in a conventional flow cell architecture, reaching near-theoretical reversible capacities at practical current rates (e.g., corresponding to 4-15 h duration stationary storage). A

lithium-polysulfide flow battery operating in both continuous-flow and intermittent-flow modes is demonstrated for the first time.

Results

The last few years have seen renewed interest in lithium-sulfur (Li-S) batteries[12–14], long considered an attractive energy storage chemistry for its high theoretical energy density (2567 Wh/kg and 2199 Wh/L for elemental Li and S as reactants) and low active materials cost. However, only recently has the adaptation of Li-S chemistry to flow batteries been considered. The high solubility of polysulfides Li_2S_x in nonaqueous electrolytes has historically been detrimental in Li-S batteries as it provides a "shuttle" mechanism for internal self-discharge[15]as well as capacity loss due to incidental Li_2S precipitation within electrochemical cells. It has been suggested that the same attributes could be exploited in flow batteries[8,9,13], with analysis indicating low storage cost ($45/kWh for the raw materials[8]) even when electrochemical cycling is limited to the solution regime between Li_2S_8 and Li_2S_4 where no precipitation occurs (Fig. 2a). In contrast to the need to minimize polysulfide solubility in a conventional Li-S electrolyte to decrease self-discharge, a high polysulfide solubility is desirable to increase the energy density and reduce the system-level cost of flow batteries. Reversible cycling has recently been demonstrated for 2.5 M to 5 M Li-PS catholyte solutions infiltrated into carbon paper current collectors against self-passivated Li metal negatives electrodes in a non-flowing "membraneless" cell configuration[8]. In the present work, we used similar Li-PS solutions in a half-flow cell against Li metal negative electrodes, the catholyte solutions being composed of Li_2S_8 dissolved in tetraethylene glycol dimethyl ether (TEGDME) containing 0.5 M bis(trifluoromethane)sulfonimide lithium salt (LiTFSI) and 1 wt. % $LiNO_3$ as the lithium

electrode passivation additive[16,17]. By starting with Li_2S_8, the sulfur precipitation regime at high charge voltage (Fig. 2a) is excluded and the starting flow electrodes have Li-PS purely in solution form. Only a microporous separator film (Tonen Chemical Corporation) separates this catholyte and the Li metal negative electrode. The theoretical specific capacity of the solution upon discharging Li_2S_8 to the Li_2S_4 liquid solution limit is 210 mAh/g, while that for discharging to Li_2S precipitation is 1460 mAh/g (Fig. 2a); at 2.5 mol S/L concentration, as used in our flow experiments, the catholyte energy density (vs. $Li^+/Li°$) is 34 Wh/L and 234 Wh/L for discharge to the solution and precipitation limits, respectively. Clearly, it is desirable to utilize storage capacity in the precipitation regime. (Herein, all specific capacities given in mAh/g refer to capacity per gram of sulfur.)

To implement the nanoconductor suspension approach, several nanoscale carbons including carbon blacks and single- and multi-wall carbon nanotubes (SWNTs and MWNTs) were dispersed in the Li-PS solution, and their conductivities and rheological properties measured, following methodologies developed in previous work on semi-solid flow batteries[5,18]. For our purposes, the ideal nanoscale conductor provides the highest electronic conductivity at the lowest volume fraction and with the lowest yield stress and viscosity. Amongst the nano-carbons tested, one particular carbon black (Ketjenblack EC-600JD, AzkoNobel, hereafter referred to as KB) met these criteria best. KB is a 1400 m^2/g nanoscale carbon with ~30nm primary particle size (TEM images in Fig. 1 and Supplementary Fig. S1). Surprisingly, electrical percolation producing 2 mS/cm electronic conductivity is observed at as low as 1 vol% KB, increasing to 9 mS/cm by 1.5 vol% carbon and 18 mS/cm by 2 vol% KB (inset of Fig. 2b). Since the room temperature ionic conductivity of the Li-PS solution is 1.5 mS/cm, the suspensions have the

unusual characteristic of being *mixed electronic-ionic conductors in fluid form*. Jamming behavior in suspensions of small particles has been studied theoretically and experimentally[19]; for instance small amplitude oscillatory shear rheometry detects mechanical percolation of micron-scale carbon particles in nonaqueous media at volume concentrations of ~5 vol%[20]. This is already much lower than the ~30 vol% percolation threshold for non-interacting like-sized spheres in three-dimensions, and has been attributed to diffusion limited aggregation (DLA) of strongly attracting particles into fractal networks (i.e., "hit and stick" behavior). The still-lower electrical percolation threshold observed here is attributed to the combination of nanoscale particle size and high ionic strength (true of any liquid electrolyte), which will further strengthen the attractive DLA interactions by quenching Debye-Huckel electrostatic double-layers that could produce interparticle repulsion. Limited tests of solutions with and without LiTFSI showed a factor of two higher dc conductivity when salt is used. Two-dimensional sections observed in wet-cell SEM (Fig 1b) are consistent with a low-density three-dimensional solids network (details appear in Supplementary Information)[21]. Viscometry showed that the 2.5 mol S/L solution has Newtonian rheology with 15 mPa s viscosity, whereas the nanoparticle suspension based on the same solvent with 1.5 vol% KB has Bingham plastic rheology with 64.6 Pa yield stress and 710 mPa-s plastic viscosity (details appear in Supplementary Information). The nanoparticle suspension has a rheological response at room temperature that is qualitatively similar to ketchup, and is readily pumped in the flow battery experiments described later.

Electrode Tests in Non-Flowing Cells. Electrochemical testing in half-cells of membraneless configuration (i.e., using only the separator film to prevent electrical contact of the two electrodes) showed that the *in-situ* nanoparticle conductor network markedly enhances the

electrochemical utilization of the polysulfide solution. Figure 2c and 2d shows direct comparisons of the same 2.5 mol S/L polysulfide solution in non-flowing half-cells with a carbon fiber current collector, and with a carbon nanoparticle suspension. The carbon fiber current collector used here and in the flow cells is a low-flow-resistance non-woven "felt" (SGL GFD3, Fig. 1c) widely used in aqueous flow batteries. For 3.0 mm-thick electrodes tested at C/50 galvanostatic rate, the capacity of the nanoparticle suspension is a factor of 4 greater than that of the conventional configuration, reaching 1000 mAh/g specific capacity. For thinner 0.5mm electrodes tested at a higher C/4 rate, the capacity of the suspension electrode reaches 1200 mAh/g (vs. 1460 mAh/g theoretical capacity), about a factor of 5 greater than with the fiber current collector. Note that the discharge curve for the Li-S system has three distinct regions (Fig. 2a). There is a high voltage plateau (~2.5 V) through which solid sulfur coexists with soluble lithium polysulfides. This is followed by a solution regime with sloping voltage (2.5-2.1 V) over which sulfur is fully dissolved as soluble polysulfides, then a lower voltage plateau (~2.0 V) where the discharge reaction proceeds via precipitation of the insoluble Li_2S. Figure 2c and 2d (showing the second cycle in all cases) show that the conventional cell architecture delivers capacity that is primarily in the solution regime. In contrast, the nanoscale suspension has both higher capacity and significantly improved reversibility when cells are cycled to include the precipitation regime. This electrode format provides correspondingly higher capacity and energy density in the same cell. It is also possible to limit cycling to the solution regime, as was done by Yang et al. using non-flowing cells with carbon paper current collectors[8]. As shown in Fig. 3, cycling of the nanoparticle suspension over the 2.55V-2.00 V solution regime gave 34% higher initial capacity than the same solution used with the carbon fiber current collector. For the suspension cycled over the solution regime, stable cycling with 56% capacity retention after 100

cycles and 50% retention after 500 cycles was seen. Cycling over the 1.90-2.50 V range to include capacity enhancement from Li_2S precipitation gave fourfold higher initial capacity of 1200 mAh/g (Fig. 3). The fade rate was also greater, yielding 610 mAh/g after 100 cycles, or about 50% retention, but this level of capacity retention is in fact superior to many published results for Li-S batteries using solid sulfur cathodes[12,13,22]. (Recent results for engineered nanostructures such as sulfur encapsulated in carbon spheres do show significantly better cycling stability[22,23].) The coulombic efficiency exceeded 95% for cycling within both the solution and precipitation regimes.

Reaction Kinetics and Contributions to Impedance. Contributions to impedance, and the origin of the highly facile reaction in the suspension electrodes, were deconvolved using electrochemical impedance spectroscopy (EIS). The Nyquist plot in Figure 2b shows the large difference in cell impedance for the two approaches, which was systematically investigated as follows. We first measured the exchange current density at the interface between carbon and the present Li-PS solutions, using carbon fiber microelectrodes and glassy carbon macroelectrodes as model current collectors. Three types of measurements, each with three-electrode cells, were conducted: 1) steady-state cyclic voltammetry at a carbon fiber microelectrode, 2) galvanostatic polarization at a glassy carbon macroelectrode, and 3) electrochemical impedance spectroscopy using a glassy carbon macroelectrode. For the present Li_2S_8 –TEGDME solutions, the three methods give exchange current densities in the range 0.011-0.030 mA cm^{-2}. Measurements of otherwise identical Li_2S_6 solutions (i.e., chemically prepared in a partially discharged state) showed ~40% higher exchange current densities, while the solution conductivity was essentially unchanged. This shows that as Li-S cells are discharged within the solution regime, the

exchange current density increases. To our knowledge these are the first exchange current density measurements for lithium-polysulfides on carbon electrodes; results are detailed in Supplementary Information.

Next, the EIS results in Fig. 2b were separated into three major impedance contributions with the help of independent measurements, using impedance spectroscopy in the absence of electrochemistry with ion-blocking (gold) electrodes, of the ionic conductivity of the Li-PS solution and the electronic conductivity of the nanoscale suspensions (inset in Fig. 2b). As shown in Table 1, the solution resistance (obtained from the high frequency intercept with the Z' axis) and interfacial resistance (the left-most arc) have similar values in the two types of cells, as expected. The difference in cell impedance is dominated by the charge transfer resistance (right-most arc), which in this case includes impedance from the finite electronic conductivity of the carbon network (whether fiber or suspension), as well as the exchange current density (Butler-Volmer kinetics) at the carbon surface. Based on the exchange current density of ~0.01 mA cm^{-2}, the actual current densities and overpotentials can be estimated as follows. The theoretically available carbon-electrolyte interfacial area of the carbon fiber current collector (Fig. 1c and Supplemental Information) is ~0.33 $m^2 g^{-1}$ based on the ~6 μm fiber diameter. The fiber current collector occupies 6 vol% of the cell, giving a collector surface area per cell volume of ~40×10^{-3} $m^2 mL^{-1}$. Figure 1c (and Supplemental Information) shows the microstructure of the 1.5 vol% KB suspension, viewed in an SEM using a "wet cell" with an electron-transparent window, and a representative primary aggregate in the dry state. The carbon nanoparticles comprise a BET area of ~1400 $m^2 g^{-1}$, which at 1.5 vol % provides carbon area per unit volume of ~42 $m^2 mL^{-1}$. Thus the available interfacial area for charge transfer is more than 10^3 greater for the suspension than

for the carbon fiber collector, even though there is only one-fourth as much carbon. Assuming all of the carbon-electrolyte interfacial area to be active, and taking the exchange current density to be 0.01 mA cm^{-2} as independently measured, discharging at a C/15 rate from composition Li_2S_8 to Li_2S corresponds to an average current density at the carbon surface of only 1.7×10^{-5} mA cm^{-2} for the nanoscale suspension, while the carbon fiber collector will need to draw 1.7×10^{-2} mA cm^{-2}. The corresponding Butler-Volmer overpotentials are 0.04 and 41.5 mV, respectively.

Further analysis of the charge transfer resistance for the nanoscale suspension suggests that at such low exchange current densities, the surface reaction kinetics may not be rate-limiting at all. If Butler-Volmer kinetics were limiting, the charge transfer resistance is computed to be 0.22 Ω cm^2 for the suspension, which is much lower than the 3.8 Ω cm^2 observed in EIS (Table 1), suggesting that the charge-transfer resistance of the nanoscale suspension is dominated by the electronic conductivity of the network. The electronic conductivity of the nanoscale suspension is ~10 mS cm^{-1} conductivity for the 1.5 vol% KB suspension (Fig. 2b), within a factor of two of that computed from the EIS charge transfer resistance assuming electronic conductivity to be the only contribution. This in turn implies that further improvements in the electronic conductivity of the nanoscale conductor suspensions could yield higher rate capability. Improvements in solution-phase ionic conductivity may also be expected to yield enhanced rate capability.

Within the precipitation regime, the poor reversibility of conventional Li-S batteries has been widely attributed to the highly insulating nature of Li_2S[24]. Here, we note that if a conformal Li_2S layer of uniform thickness is assumed to form on the carbon surface during full discharge from

Li_2S_8 to Li_2S, at 2.5 mole S/L concentration the layer thickness (based on a molar volume of $2.768x10^{-2}$ L/mol for Li_2S[25]) is 1.7 nm for the nanoscale suspension, compared to 1.7 μm for the carbon felt current collector. Thus the superior capacity and reversibility of the nanoscale suspension can be attributed to a combination of two effects: ultra-low current densities at the catholyte-carbon interface, and a much finer-scale precipitation of Li_2S. Topologically, the embedded, self-healing current collector is in some ways the inverse of the mesoporous carbon hosts for sulfur that have shown promise in conventional Li-S batteries[26]. The current conductive, flowable electrode approach may have benefits for non-flowing metal-sulfide batteries as well, as illustrated by the cell results in Figs. 2c and 2d.

Flow Cell Tests. Tests performed in a lab-scale half-flow cell (Fig. 1b) showed that the vastly improved charge transfer kinetics of the nanoscale suspensions are retained under two types of flowing conditions: 1) continuous flow, which is the typical operating mode of solution-based flow batteries; and 2) intermittent flow, where fluid is pumped in discrete volumes with complete charging or discharging of the electroactive region occurring in between. Intermittent flow has been shown to produce higher round-trip energy efficiency for significantly non-Newtonian redox fluids[5,27,28].

To demonstrate cycling under continuous flow, automated digitally-controlled syringe pumps were used with the cell in Fig. 1b. The ratio of cell volume to pumped volume was 1:4, and the total volume (80 μL) passes through the cell in 100 min. (i.e., for a flow battery with a single cathode tank, the entire tank volume would circulate once every 100 min.) Results for the nanoscale suspensions appear in Fig. 4. During the first 1.5 cycles, the cell was discharged and

charged potentiostatically between 2.1 V and 2.5 V (Fig. 4) to stay in the solution regime, similar to Yang et al.'s experiments[8]. Supplementary Movie S1 depicts a simulation (details described in SI) of the time-dependent continuous-flow protocol for cycling in this regime. Since the Li-PS battery is assembled in the charged state, the first half-cycle discharges the cell, whereas the relevant coulombic and energy efficiency for a storage battery is that occurring upon charging and discharging. Efficiencies are therefore only reported for subsequent cycles where there is a full charge/discharge sequence. During the potentiostatic charge/discharge cycle in the solution regime, the discharge capacity is 181mAh/g, the coulombic efficiency is 101% (the higher-than-theoretical value is due to diffusive exchange of charged cathode at the edges of the electroactive zone), and the round-trip energy efficiency is 84.7%. Operating in this regime, the energy density of the flow cathode alone is 30.4 Wh/L (specific energy 380 Wh/kg). To evaluate the energy density of the electrochemical couple, a reasonable excess of Li metal must be assumed. Herein we will assume 100% excess of Li relative to the actual capacity of the cell, in which case the active-materials-only energy density in the solution regime is 26.7 Wh/L (specific energy 334 Wh/kg).

A stepped potentiostatic protocol was then applied between voltage limits of 2.5 V-1.6 V, as shown for the intermediate cycles in Fig. 4. This cycles the flow cathode into the precipitation regime, more than doubling the capacity compared to the solution regime. The step sequence was selected to provide approximately constant overpotential relative to the equilibrium cell voltage; more sophisticated feedback-based control algorithms that control overpotential are clearly possible. For the third complete charge/discharge cycle, the discharge capacity is 393 mAh/g, and coulombic and energetic efficiencies are 95.6% and 75.7%, respectively. Under this

potentiostatic protocol, the net cycling rate for the entire system is C/15 on charge and C/22 on discharge. The cathode discharge energy density is 61 Wh/L (760 Wh/kg), and the cathode plus lithium energy density is 46.7 Wh/L (584 Wh/kg). Finally, the cell was cycled potentiostatically between the same voltage limits, but without intermediate potential steps. This increases the system-level C-rate to C/10 for charge and C/15 for discharge, and correspondingly, the capacity is slightly lower at 376 mAh/g in cycle 5, and energy efficiency decreases to 63%. The reduced energy efficiency is to be expected for this potentiostatic protocol due to the high overpotential relative to equilibrium cell voltage that is applied across most of the state of charge range. The active-materials-only discharge energy density is 44.1-48.1 Wh/L (552-602 Wh/kg). During cycles 5-14, despite some capacity fade as shown in the inset in Fig. 4, the coulombic efficiency remains above 99.5%. This suggests that impedance growth rather than loss of storage capacity in the flow cathode is responsible for the capacity fade. It would not be surprising for impedance growth to take place at the stationary Li metal negative electrode, given the large areal capacity that is reversibly plated throughout this experiment. Upon increasing charge time by ~10% in cycle 15 (not shown), we found that the discharge capacity was restored, consistent with an impedance limitation.

Intermittent flow cycling was then demonstrated using the same cell geometry and nanocarbon suspension, with results appearing in Fig. 5. Optimization for efficiency in the intermittent flow protocol has been discussed in detail in recent work.[7,28] A total of five cell volumes was flowed through the cell during a complete charge-discharge cycle, with each flow pulse having a volume that is one-half the cell volume (i.e., ten intermittent pumping pulses were used during each discharge and charge). Fluid-mechanical analysis (see Supplementary Information) suggests that

the velocity profile in the flow cell is highly non-uniform, based on the suspension's rheology, pulse flow rate (30 μL/s), and channel design[28]. Accordingly, the volume of intermittent flow pulses was chosen to minimize the coulombic and energetic inefficiencies that are induced by flow non-uniformity. After each pumping step, the cell was galvanostatically discharged or charged, testing the solution and precipitation regimes with voltage limits of 2.55 V-1.95 V and 2.8 V-1.6 V, respectively. The capacity axis in Fig. 5 gives the specific capacity with respect to all sulfur in the system, assuming a uniform state-of-charge.

Fig. 5a shows the discharge-charge curve for the solution-only case, where the discharge and charge capacities are 162 mAh/g and 172 mAh/g, respectively, and the total discharge rate for the tank is C/5. The voltage-efficiency under these conditions (84 % at C/5) exceeds that of potentiostatic, continuous-flow cycling at lower effective rate (78 % at ~C/10). This performance demonstrates the ability of the intermittent flow mode to cycle more efficiently than continuous flow. The simulated charge-discharge curve under these conditions is shown in Fig. 5b, following the model of Smith et al. with details appearing in the SI[28]. The simulated state-of-charge evolution during the intermittent flow sequence is shown in Supplementary Movie S2. The discharge voltage trends of the experiment and simulation agree well. An instantaneous jump in discharge voltage occurs after each intermittent flow pulse, because fresh suspension, rich in Li_2S_8, flows into the cell's electroactive region. The value of the voltage after the pulse (2.1-2.2 V) is substantially less than the open-circuit potential of the Li_2S_8 suspension (2.42 V). Voltage is reduced below this value because the electroactive region is incompletely replenished by the flow pulse[7,28]. As a result, the solution phase of the suspension is more highly charged near the cell's inlet (nominally, Li_2S_8) than near the outlet (nominally, Li_2S_4). The average

discharge voltage of the experiment (2.06 V) is in excellent agreement with the simulation (2.07 V), suggesting that Li-PSs are locally in equilibrium during discharge, as assumed in the model. The experimental charge-voltage trends differ markedly from the idealized model, though, with a 70 mV deviation on average. While the simulation predicts linear variation of voltage with time after an intermittent pulse, the experiment exhibits sigmoidal variation of voltage. Recent *in operando* analyses of speciation in Li-S systems have suggested that charge and discharge processes in the Li-S system proceed through different reaction pathways[29]. The present deviation of experimental charge voltage from the simulation is consistent with these observations.

When the voltage window is widened to include precipitation, the discharge capacity is increased about four-fold to 653 mAh/g (Fig. 5c), with the discharge rate decreasing to C/18. These initial results demonstrate what we believe to be a higher efficiency alternative to continuous flow mode operation that reduces pumping losses, especially for higher energy density redox electrodes with substantial yield stresses and strongly shear-thinning rheology.

Thus we show that by using nanoscale conductor suspensions to form flowable electrically percolating networks, the electrochemical reactivity of solution-based redox electrodes can be greatly enhanced compared to that obtained with a conventional carbon fiber current collector. In addition, this novel flow electrode architecture allows redox solutions to be reversibly cycled into composition regimes where solid precipitation occurs. The nanoscale suspensions retain their electronic conductivity and enhanced reactivity under flow, and can be regarded as "self-healing." They may be used in flow cells that operate in continuous or intermittent flow modes.

Just 1.5 vol% added nanoscale carbon allows Li-PS flow electrodes to operate in the precipitation regime where the specific energy and energy density increase by up to a factor of 5 compared to that obtained using only the solution regime. One of the great attractions of the Li-S system is the very low cost of the elemental reactants on an energy basis. For a reversible capacity of 600 mAh/g and average discharge voltage of 1.9V representing the present 2.5 mol S/L system, the raw materials cost of the flow cathode is $21/kWh, and that of the electrochemical couple (assuming 100% excess of Li metal) is only $37/kWh, leaving ample room for other component cost while meeting the $100/kWh target. We believe that with further development, higher capacity utilization in higher molarity solutions is achievable, which would further drive down the cost of storage. The nanoconductor suspension architecture can clearly also be used for anolytes, allowing a full flow battery as well as the half-flow system demonstrated here.

Methods:

Preparation of flow electrodes

To prepare the lithium polysulfide solution, Li_2S, sulfur, LiTFSI, and $LiNO_3$ were dried under vacuum for 24 h at 100 ºC and added to TEGDME and stirred for 24 h in an Ar-filled glovebox, at 60ºC. To prepare the suspension, carbon black (KetjenblackEC-600JD, AzkoNobel) was added to the aforementioned solution, manually stirred, and then sonicated for 30 minutes. LiTFSI and $LiNO_3$ were obtained from Sigma-Aldrich, while the sulfur, Li_2S, and TEGDME were obtained from Alfa Aesar.

Microscopy Characterization

Scanning electron microscopy of the carbon felt was carried out using a FEI/Philips XL30 environmental SEM with secondary electron detector operating at 25 kV accelerating voltage. Suspensions were imaged in QuantomiX WETSEM® QX-102 capsules using the FEI/Philips XL30 with a backscattered electron detector and accelerating voltages of 20-30 kV. The dry Ketjenblack powder was imaged on a JEOL 2010F transmission electron microscope with an accelerating voltage of 200 kV. Samples were prepared by dispersing the carbon black on a Cu grid coated with an amorphous carbon film.

Exchange current density measurements

In the galvanostatic polarization experiment, the polysulfide solution was vigorously stirred to ensure no mass-transport limitation, while a specified current was drawn from the cell using a 3 mm glassy carbon working electrode (CH Instruments, Inc.) for 30 minutes. The corresponding potential was determined as the average potential during the 30 minute galvanostatic step. In the steady-state voltammetry experiments, an 11 μm carbon-fiber microelectrode (BASi, Inc) was used as a working electrode and the potential was swept cathodically at 20 mV/s from 3.24 V vs. Li^+/Li to 1.24 V.

Cycling experiments in non-flowing half-cells

Swagelok® type cells with 0.5 mm deep wells were used. A Tonen separator soaked with electrolyte was used. All cell assembly was performed inside an argon-filled glovebox.

Flow cell experiments

The lab-scale flow cell used for intermittent and continuous flow experiments was machined from polyvinylidene fluoride (PVDF), with an electroactive region machined from nickel and sputter-coated with gold. The electroactive region was 20 mm long, with square cross sections ranging from 1 mm to 2.8 mm width. For a 1 mm channel, the channel volume was 20 μL, with

an active membrane area of 0.2 cm^2. The cell was connected with polytetrafluoroethylene (PTFE) tubing to gastight glass syringes (Hamilton Model 1005), which were driven using syringe pumps (neMESYS, Cetoni GmbH). Electrochemical testing was performed using a Bio-Logic potentiostat.

EIS and IS measurements

Electrochemical impedance measurements were made in Swagelok-type cells (Swagelok Co.) with a PTFE body, cathode well 6.35 mm in diameter and 2.8 mm deep, and with Li metal as a counter and reference electrode. The measurements were taken with Li_2S_8 solutions, 2.5 mol S L^{-1} in TEGDME with 0.5 M LiTFSI supporting electrolyte. The suspension has 1.5 vol% Ketjenblack. The well is Au coated Ni. When characterizing the solution electrode, 3 mm thick carbon felt was cut to fit the cathode well and compressed to 2.8 mm thickness upon assembly. When measuring the suspension electrodes, the suspensions were spatula-loaded into the well and covered with a circular piece of separator film. A circular film of lithium metal, attached to a stainless steel current collector, was applied against the well by light spring force. IS electronic and ionic conductivity measurements were made in a similar two-electrode cells using gold-sputtered current collectors on both sides. Measurements were taken over the course of one to two hours.

The EIS measurements used the Solartron 1400 system with a Solartron 1455 frequency response analyzer. The experiments were performed in with cells in the fully charged (as-assembled) state. Sinusoidal voltage oscillations of 10 mV amplitude were applied about the cell's open circuit voltage between the two electrodes. Oscillation frequencies were swept logarithmically from 0.01 Hz to 1MHz. The measured impedance data were fit to an equivalent circuit by a complex nonlinear least squares regression. For the IS measurements, a Solartron

Analytical model 1470 potentiostat and model 1455 frequency response analyzer were used to apply either a +/-50 mV AC or DC bias. The DC measurements were taken at a steady state value after a 15 minute hold. Resistances were converted to conductivities by dividing by the experimental cell factor, calibrated to be 1.2 cm^{-1} using a 15 mS/cm conductivity standard produced by Oakton Instruments.

Rheological characterization

The viscometric behavior of the different solutions and semi-solid suspensions was measured using a Malvern Kinexus Pro torsional rheometer enclosed in a glovebox with an Argon atmosphere (H_2O & O_2 levels < 0.1 ppm). Steady shear viscometry tests, as well as, small amplitude oscillatory frequency sweeps, were performed using a smooth parallel plate geometry (D = 40 mm; mean roughness $R_q = 0.36\ \mu m$). All tests were performed at T = 25°C and the temperature was regulated with a Peltier plate system. Steady shear tests were performed with decreasing applied shear rates as described by Ovarlez et al.[30] to insure the existence of a simple yield stress for the material and avoid possible transient shear banding. In addition, following the protocol proposed by Yoshimura & Prud'Homme[31], the same sample was tested at three different gaps (H = 1 mm, 0.75 mm, 0.5 mm respectively) to probe and correct for slip effects. If the flow curves at different gaps superimpose, the material does not slip. If gap-dependent rheology is observed, a correction needs to be applied to extract the true shear rate applied on the sample at each value of the applied stress.

Author contributions:

F.Y.F. and Z.L. developed the electrode compositions and conducted the electrochemical cell tests. W.H.W. conducted the electron microscopy, carried out exchange current density measurements, and interpreted the rate-limiting mechanisms. K.C.S. and W.C.C. modeled and

interpreted the flow cell data. N.B. measured suspension and cell electrical properties. A.H. and G.H.M. measured and interpreted flow electrode rheology. Y.-M.C. conceived of and supervised the project and wrote the first draft of the manuscript.

Competing financial interests

The authors declare no competing financial interests.

References

1. Dunn, B., Kamath, H. & Tarascon, J.-M. Electrical energy storage for the grid: a battery of choices. *Science* **334,** 928–35 (2011).

2. Yang, Z. *et al.* Electrochemical energy storage for green grid. *Chem. Rev.* **111,** 3577–613 (2011).

3. ARPA-E FOA# DE-FOA-0000290: Grid-Scale Rampable Intermittent Dispatchable Storage (GRIDS). at <https://arpa-e-foa.energy.gov/FoaDetailsView.aspx?foaId=85e239bb-8908-4d2c-ab10-dd02d85e7d78>

4. Weber, A. Z. *et al.* Redox flow batteries: a review. *J. Appl. Electrochem.* **41,** 1137–1164 (2011).

5. Duduta, M. *et al.* Semi-solid lithium rechargeable flow battery. *Adv. Energy Mater.* **1,** 511–516 (2011).

6. Hamelet, S. *et al.* Non-aqueous Li-based redox flow batteries. *J. Electrochem. Soc.* **159,** A1360–A1367 (2012).

7. Li, Z. *et al.* Aqueous semi-solid flow cell: demonstration and analysis. *Phys. Chem. Chem. Phys.* **15,** 15833 (2013).

8. Yang, Y., Zheng, G. & Cui, Y. A membrane-free lithium/polysulfide semi-liquid battery for large-scale energy storage. *Energy {&} Environ. Sci.* **6,** 1552 (2013).

9. Demir-Cakan, R., Morcrette, M., Guéguen, A., Dedryvère, R. & Tarascon, J.-M. Li–S batteries: simple approaches for superior performance. *Energy Environ. Sci.* **6,** 176 (2013).

10. Brushett, F. R., Vaughey, J. T. & Jansen, A. N. An all-organic non-aqueous lithium-ion redox flow battery. *Adv. Energy Mater.* **2,** 1390–1396 (2012).

11. Pratt III, H. D., Rose, A. J., Staiger, C. L., Ingersoll, D. & Anderson, T. M. Synthesis and characterization of ionic liquids containing copper, manganese, or zinc coordination cations. *Dalt. Trans.* **40,** 11396 (2011).

12. Bruce, P. G., Freunberger, S. A., Hardwick, L. J. & Tarascon, J.-M. Li--O2 and Li--S batteries with high energy storage. *Nat. Mater.* **11,** 19–29 (2012).

13. Manthiram, A., Fu, Y. & Su, Y.-S. Challenges and prospects of lithium--sulfur batteries. *Acc. Chem. Res.* **46,** 1125–1134 (2013).

14. Van Noorden, R. Sulphur back in vogue for batteries. *Nature* **498,** 416–417 (2013).

15. Mikhaylik, Y. V. & Akridge, J. R. Polysulfide shuttle study in the Li/S battery system. *J. Electrochem. Soc.* **151,** A1969 (2004).

16. Mikhaylik, Y. V. Electrolytes for lithium sulfur cells. U.S. Patent 7,352,680. (2008).

17. Aurbach, D. *et al.* On the surface chemical aspects of very high energy density, rechargeable Li-sulfur batteries. *J Electrochem Soc* **156,** A694–A702 (2009).

18. Ho, B. Y. An experimental study on the structure-property relationship of composite fluid electrodes for use in high energy density semi-solid flow cells. Ph.D. Thesis. Massachusetts Institute of Technology. (2012).

19. Osuji, C. O., Kim, C. & Weitz, D. a. Shear thickening and scaling of the elastic modulus in a fractal colloidal system with attractive interactions. *Phys. Rev. E* **77,** 060402 (2008).

20. Trappe, V. & Weitz, D. Scaling of the viscoelasticity of weakly attractive particles. *Phys. Rev. Lett.* **85,** 449–52 (2000).

21. Bird, R. ., Dal, G. C. & Yarusso, B. J. The rheology and flow of viscoplastic materials. *Rev. Chem. Eng* **1,** 1–70 (1982).

22. Bresser, D., Passerini, S. & Scrosati, B. Recent progress and remaining challenges in sulfur-based lithium secondary batteries--a review. *Chem. Commun. (Camb).* **49,** 10545–62 (2013).

23. Zhang, B., Qin, X., Li, G. R. & Gao, X. P. Enhancement of long stability of sulfur cathode by encapsulating sulfur into micropores of carbon spheres. *Energy Environ. Sci.* **3,** 1531 (2010).

24. Yang, Y. *et al.* High-capacity micrometer-sized Li 2S particles as cathode materials for advanced rechargeable lithium-ion batteries. *J. Am. Chem. Soc.* **134,** 15387–15394 (2012).

25. Kumaresan, K., Mikhaylik, Y. & White, R. E. A mathematical model for a lithium–sulfur cell. *J. Electrochem. Soc.* **155,** A576–A582 (2008).

26. Ji, X., Lee, K. T. & Nazar, L. F. A highly ordered nanostructured carbon--sulphur cathode for lithium--sulphur batteries. *Nat. Mater.* **8,** 500–506 (2009).

27. Brunini, V. E., Chiang, Y.-M. & Carter, W. C. Modeling the hydrodynamic and electrochemical efficiency of semi-solid flow batteries. *Electrochim. Acta* **69,** 301–307 (2012).

28. Smith, K. C., Chiang, Y.-M. & Carter, W. C. Maximizing energetic efficiency in flow batteries utilizing non-Newtonian fluids. In review. (2013).

29. Cuisinier, M. *et al.* Sulfur speciation in Li–S batteries determined by operando X-ray absorption spectroscopy. *J. Phys. Chem. Lett.* **4,** 3227–3232 (2013).

30. Ovarlez, G., Cohen-Addad, S., Krishan, K., Goyon, J. & Coussot, P. On the existence of a simple yield stress fluid behavior. *J. Nonnewton. Fluid Mech.* **193,** 68–79 (2013).

31. Yoshimura, A. N. N. & Prud'Homme, R. K. Wall Slip Corrections for Couette Disk Viscometers and Parallel. *J. Nonnewton. Fluid Mech.* **32,** 53–67 (1988).

Figure Captions

Figure 1. Conventional flow battery vs. new scheme. (a) Flow batteries combine a current-extracting stack, through which redox active solutions flow, with storage tanks and pumps. In conventional flow batteries the electrodes are electronically insulating fluids that react only upon charge transfer to porous current collectors typically based on carbon or metals. (b) Laboratory

half-flow cell used in current work to compare (c) Conventional flow cell architecture using stationary carbon fiber current collector, with (d) New scheme providing electronically conductive flowing redox electrodes based on nanoscale percolating networks of conductor particles forming an embeded, self-healing current collector. The mixed-conducting fluid allows charge transfer reactions throughout volume of flow electrode.

Figure 2. (a) The Li-sulfur reaction upon discharge proceeds by the lithiation of elemental S_8, followed by a regime of soluble polysulfides between compositions Li_2S_8 and Li_2S_4, then the precipitation of Li_2S. Attaining high specific capacity requires precipitation of Li_2S. In this work, starting solutions containLi_2S_8 and were discharged within and beyond the solution regime, respectively. (b) Electrochemical impedance spectroscopy comparing cells with identical 2.5 mol S/L solutions (as Li_2S_8 in TEGDME with 1 wt% $LiNO_3$ with 0.5M LiTFSI) in the conventional architecture with carbon felt current collector and the nanoscale conductor suspension (1.5 vol% KB). A much smaller charge-transfer resistance (leftmost red arc) is seen for the latter. (c) and (d) Four- to fivefold higher reversible capacity is seen for the nanoscale conductor suspension over the conventional flow cell design when cycling over 2.5-1.6V to include the precipitation regime, in both 3.0 mm and 0.5 mm thick electrodes. Charge-discharge curves are the second galvanostatic cycle for each cell.

Figure 3. Charge and discharge capacity vs. cycle number, at C/4 rate, for non-flowing half-cells containing as cathode the nanoscale suspension flow cathode and the solution alone with carbon fiber current collector). The 2.50-2.00V range permits only polysulfide solutions, while the 2.50-1.90V window incorporates Li_2S precipitation. All cells use the same 2.5 mol S/L starting

solution. The nanoscale suspension cycled over solution + precipitation regimes exhibits 1200 mAh/g initial capacity (1460 mAh/g theoretical value) with capacity retention comparable to the state-of-art conventional Li-S cells. When cycled over the polysulfide solution regime, the nanoscale suspension flow electrode shows ~34% higher initial capacity than the conventional architecture.

Figure 4. Continuous flow cell operation under potentiostatic cycling protocols, for nanoscale suspension electrode (2.5 mol S/L) in half-flow cell of Fig. 1b. Initial 1.5 cycles correspond to cycling over 2.5-2.1V, within polysulfide solution regime. Subsequent three cycles have stepped voltage protocol maintaining approximately constant overpotential over 2.5-1.6V, inducing Li_2S precipitation. Cycles 5-14 have potentiostatic holds at 2.5V upon charge and 1.6V upon discharge. Capacity vs. cycle number are shown in inset figure. Coulombic efficiencies averaged ~99% throughout while energy efficiencies varied with protocol as discussed in text.

Figure 5. Intermittent flow cell operation with galvanostatic protocols, for nanoscale suspension electrode (2.5 mol S/L) in half-flow cell of Fig. 1b. Total volume pumped through cell is five times the cell internal volume (5:1 tank:stack ratio), and is pumped one-half of a cell volume per stroke. The capacity axis gives the specific capacity with respect to all sulfur in the system, assuming a uniform state-of-charge. (a) Galvanostatic discharge to 1.95V, and charge to 2.55V, to remain within polysulfide regime. Discharge rate is C/5 for total system. (b) Simulation of experiment in (a) using model described in Supplementary Information. (c) Galvanostatic discharge to 1.6V and charge to 2.55V, to include Li_2S precipitation with concommittent higher capacity. Net discharge rate is C/18. See text for discussion.

Sample	Solution Resistance (Ω cm^2)	Interfacial Resistance (Ω cm^2)	Charge Transfer Resistance (Ω cm^2)
Nanoconductor Suspension	5.1	16	3.8
Carbon Fiber Current Collector	3.5	31	125

Table 1: Comparison of impedance contributions for non-flowing Li/polysulfide cells using the same Li-PS solution with a nanoscale conductor suspension and with a conventional carbon fiber current collector.

Figures

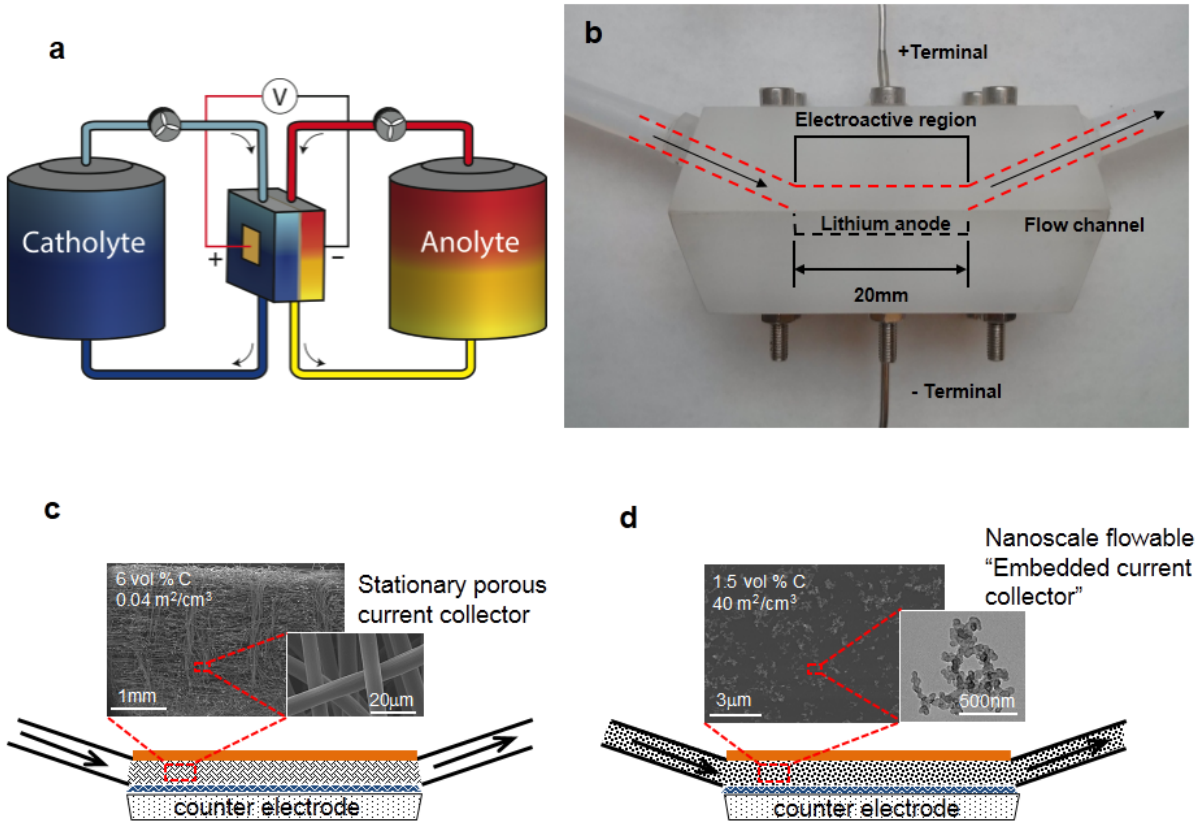
a
V
Catholyte
Anolyte
+
–
b
+Terminal
Electroactive region
Lithium anode
Flow channel
20mm
- Terminal
c
6 vol % C
0.04 m²/cm³
1mm
20µm
Stationary porous
current collector
counter electrode
d
1.5 vol % C
40 m²/cm³
3µm
500nm
Nanoscale flowable
"Embedded current
collector"
counter electrode

Figure 1

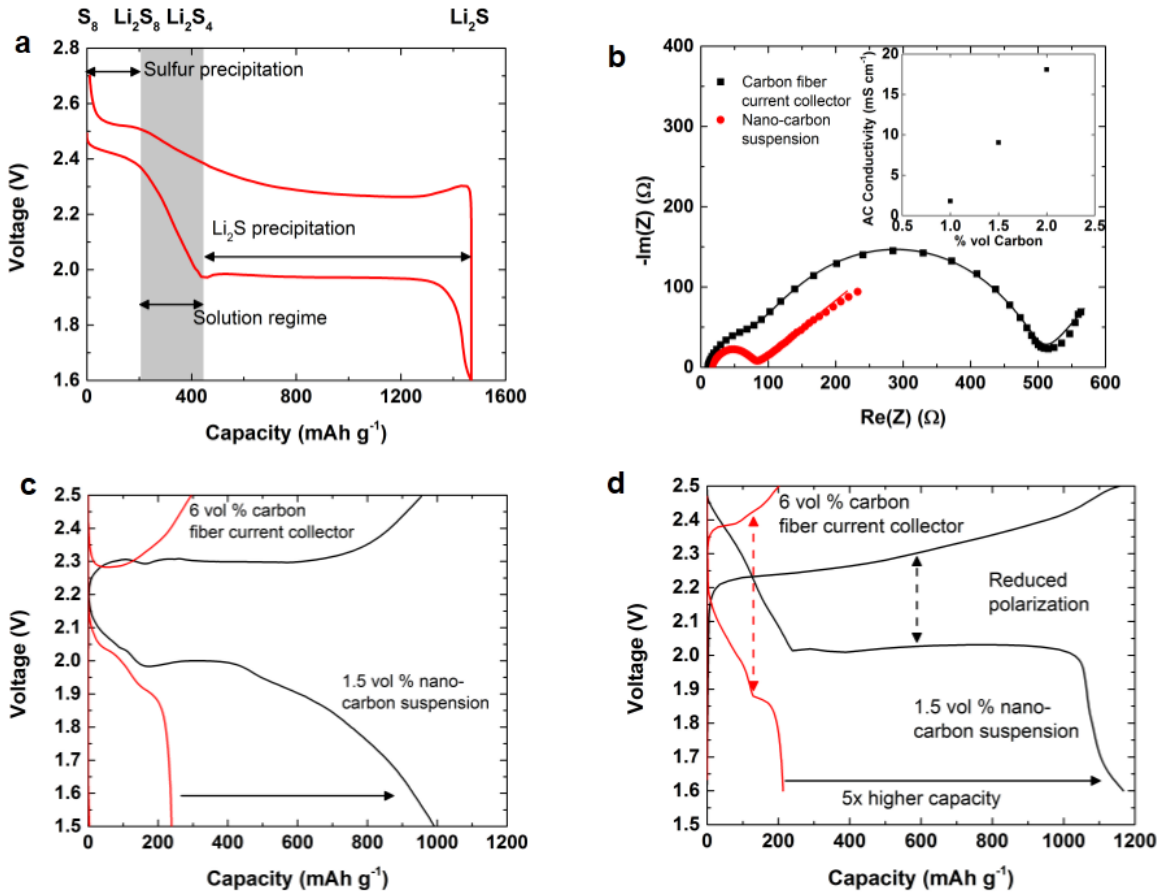
a
S8 Li2S8 Li2S4
Li2S
Sulfur precipitation
Li2S precipitation
Solution regime
Voltage (V)
Capacity (mAh g-1)
b
Carbon fiber current collector
Nano-carbon suspension
-Im(Z) (Ω)
Re(Z) (Ω)
AC Conductivity (mS cm-1)
% vol Carbon
c
6 vol % carbon fiber current collector
1.5 vol % nano-carbon suspension
Voltage (V)
Capacity (mAh g-1)
d
6 vol % carbon fiber current collector
Reduced polarization
1.5 vol % nano-carbon suspension
5x higher capacity
Voltage (V)
Capacity (mAh g-1)

Figure 2

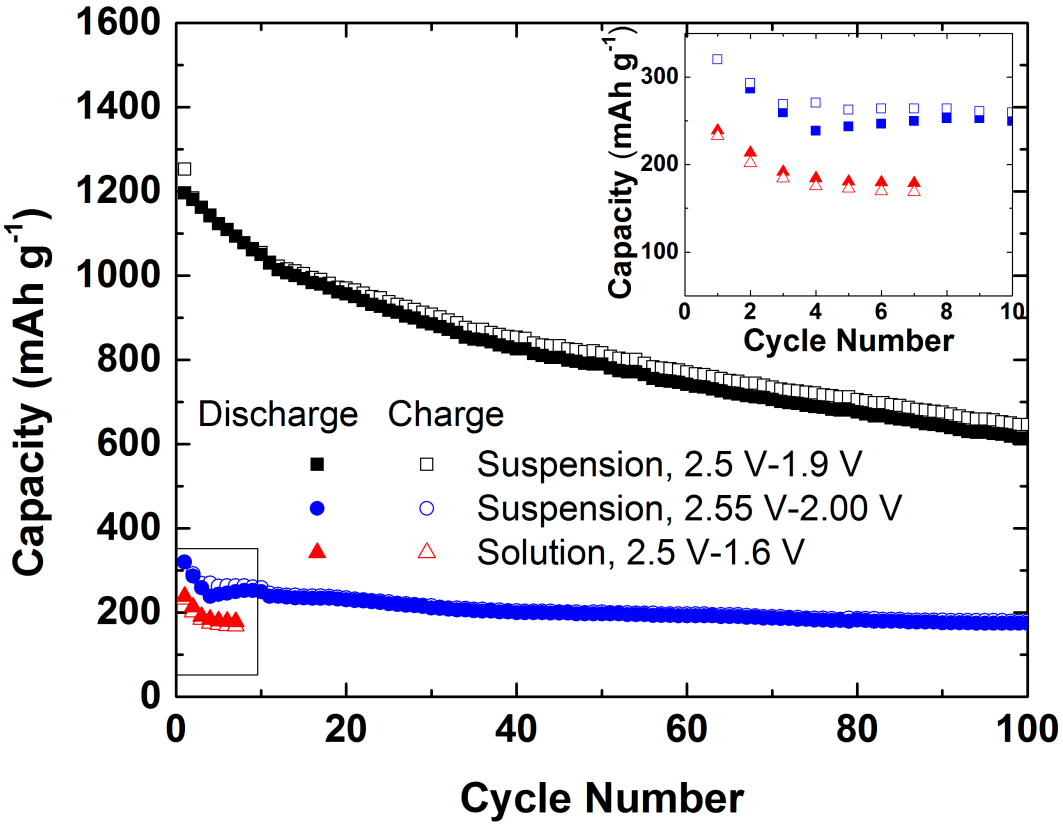
Capacity (mAh g-1)
Cycle Number
Discharge
Charge
Suspension, 2.5 V-1.9 V
Suspension, 2.55 V-2.00 V
Solution, 2.5 V-1.6 V
Capacity (mAh g-1)
Cycle Number

Figure 3

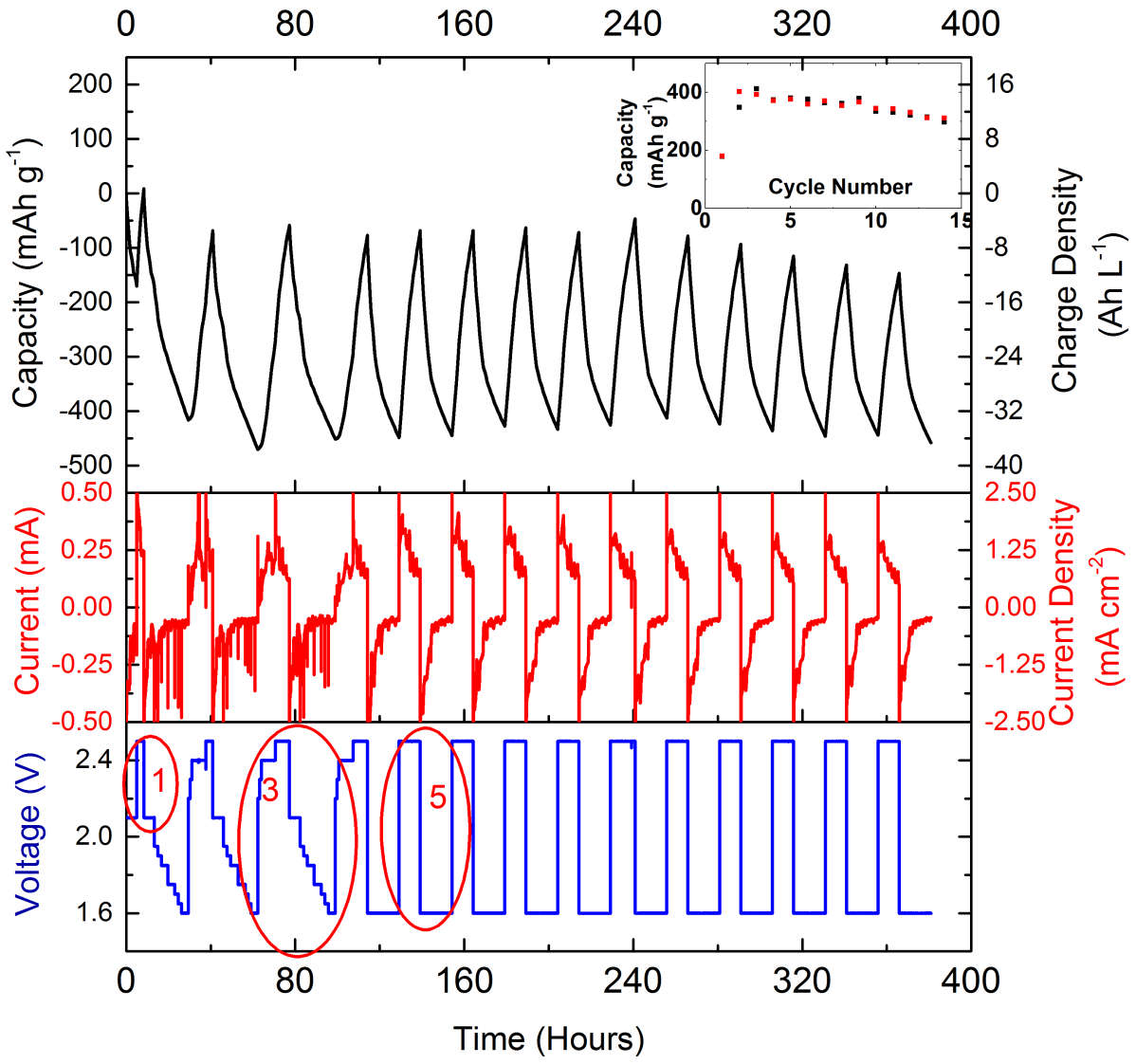
Capacity (mAh g-1)
Charge Density (Ah L-1)
Current (mA)
Current Density (mA cm-2)
Voltage (V)
Time (Hours)
Capacity (mAh g-1)
Cycle Number
1
3
5

Figure 4

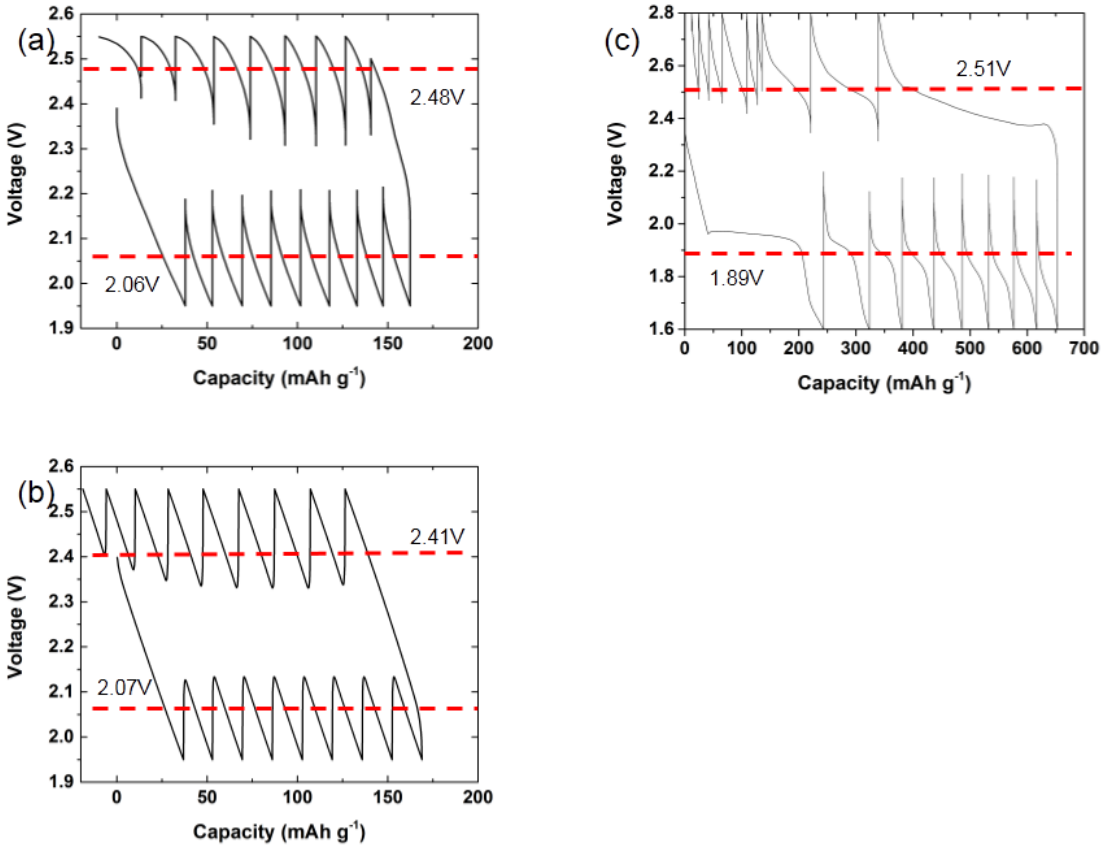
(a)
2.48V
2.06V
Voltage (V)
Capacity (mAh g-1)
(b)
2.41V
2.07V
Voltage (V)
Capacity (mAh g-1)
(c)
2.51V
1.89V
Voltage (V)
Capacity (mAh g-1)

Figure 5